X-615-68-285
PREPRINT

NASA TM X- 63345

THE INFLUENCE OF VARYING SOLAR FLUX ON IONOSPHERIC TEMPERATURES AND DENSITIES: A THEORETICAL STUDY

J. R. HERMAN
S. CHANDRA

JULY 1968

GSFC — GODDARD SPACE FLIGHT CENTER
GREENBELT, MARYLAND

THE INFLUENCE OF VARYING SOLAR FLUX ON IONOSPHERIC TEMPERATURES AND DENSITIES: A THEORETICAL STUDY*

by

J. R. Herman and S. Chandra
Laboratory for Space Sciences
NASA Goddard Space Flight Center
Greenbelt, Maryland

ABSTRACT

The electron continuity equation and the heat conduction equations for electrons, ions, and neutral species are solved simultaneously for specified boundary conditions and values of the solar flux. These solutions have yielded a set of self-consistent steady state profiles for a variety of midday solar conditions that are in agreement with observational data. To produce these profiles only the boundary conditions and solar flux are used as variable parameters of the problem. It is shown that the neutral temperature and the resulting neutral gas composition play a dominant role in determining the charged particle density and temperature profiles. This leads to a picture of the solar cycle variation where composition changes in the neutral gas (introduced at the lower boundary) must be combined with the solar flux variation to produce physically reasonable results. Of the five neutral gases used, (N_2, O_2, O, He, H) the atomic oxygen density variations are shown to be most effective in producing the observed trends for all the temperatures and densities in the E and F regions.

*To be published in PLANETARY AND SPACE SCIENCE

INTRODUCTION

The importance of obtaining a simultaneous solution of the equations of continuity, momentum, and heat transport for the electron, ion, and neutral gases has been recognized for some time. The processes influencing the general behavior of the E and F regions arising from changes in solar activity have a strong interdependence. A change in solar EUV radiation directly alters the photoionization rate and photoelectron energy spectrum. These in turn produce a sequence of secondary or indirect effects whose influence on the ionosphere is quite complex. For example, a fraction of the solar EUV radiation is absorbed by the neutral atmosphere and transformed into internal energy. The release of this energy by super-elastic collisional heating results in composition and temperature changes of the ionizable constituents; thus indirectly effecting the photoionization rate. The charged particle loss and transport processes are similarly effected by a series of cyclic chain reactions involving density, composition, and temperature of all the ionospheric constituents. Figure 1 shows a rough schematic illustrating the basic coupling between the various components making up the ionospheric system. In solving the equation of continuity or heat transport it has been usual to assume a suitable model for the unknown quantities appearing in the equations. This approach, while quite useful in under-

standing the general physical processes governing the E and F regions, masks the essential processes needed for studying the behavior due to changes in solar activity.

The recent largely successful effort to make simultaneous measurements of the temperatures and densities of the ionizable and neutral constituents in the E and F regions (Geoprobe), has increased the importance of obtaining a corresponding simultaneous theoretical description for the upper atmosphere. It is hoped that a clearer understanding of the cause and effect relationships can be obtained through such an effort.

In this work a simultaneous solution is described of the continuity and heat conduction equations for an ionospheric plasma consisting of electrons, atomic oxygen ions, and the neutral gas species N_2, O_2, O, He, and H. The solutions are presented for steady state conditions obtained by integrating the time dependent differential equations with time independent driving functions (stationary sun) until the transients introduced by the arbitrary choice of initial conditions vanish.

Various studies have been conducted based on these equations [see Rishbeth (1968), Yonezawa (1966), and Evans (1966) for general references], using slightly modified forms of the transport coefficients described in the earlier works of Chapman (1952), Nicolet (1961), and Spitzer (1965). More recently Dalgarno et. al. (1963) and Banks (1966) have listed many of the detailed expressions for the transport coefficients and driving functions

used in the ionosphere. Even though each of these works essentially analysed a single equation, the results demonstrate that the equations are sufficient to account for many features of the ionospheric plasma.

In this paper we have followed the forms of the equations as given by Harris and Priester (1962) for the neutral temperature, Shimizaki (1965) for the electron continuity equation, and Banks (1966) for the charged particle temperatures. Because of these earlier works only an outline of the equations is presented instead of the detailed derivations.

ELECTRON TEMPERATURE

In order to describe the electron temperature profiles for various solar conditions it is necessary to consider the dominant effects of heat conduction and net local heat production. These effects correctly give the magnitude and shape of the temperature profile throughout the region of interest for midday conditions. Other terms can be included in the heat conduction equation to further refine the model, such as the effect of convection and non-local heating. However, such refinements have little effect on the steady state solutions and their interpretations as presented here. On the other hand, many of the interesting features of the diurnal behavior of the ionosphere arise from the inclusion of these extra terms.

Accordingly, the following form of the heat conduction

equation is used for the electron temperature.

$$n_e k C_v \frac{\partial T_e}{\partial t} - \nabla \cdot [K_e \nabla T_e] = Q_e - L_e \qquad (1)$$

If the main heat flow is along the earth's magnetic field lines, and if the flat earth approximation is used, then in terms of the altitude z, the time t, and the magnetic dip angle I, the electron temperature profile $T_e(z)$ is given by [Geisler and Bowhill (1965)]

$$n_e k C_v \frac{\partial T_e}{\partial t} - \sin^2 I \frac{\partial}{\partial z} [K_e \frac{\partial T_e}{\partial z}] = Q_e - L_e \qquad (2)$$

where K_e = the electron thermal conductivity

n_e = the electron density (cm^{-3})

k = Boltzmann's constant = 1.38×10^{-16} ergs/^oK

C_v = the specific heat of the electron gas at a constant volume

Q_e = the electron heat production rate

L_e = the electron heat loss rate

The electron heat conductivity is based on Spitzer's formulation for a fully ionized Lorentz gas modified to account for the reduced electron mean free path due to the presence of the neutral gases. The main result of the modification is to reduce the effective thermal conductivity and increase the coupling to the neutral gas at lower altitudes. From Spitzer and Härm (1953) the thermal conductivity is given by

$$K_e^{(s)} = 1.23 \times 10^{-6} T_e^{5/2} \text{ ergs cm}^{-1}\text{sec}^{-1} {}^oK^{-1} \qquad (3)$$

Introducing the modifications to account for the reduced mean free path

$$K_e = \left[\frac{1}{K_e(s)} + \sum_n \frac{1}{K_e^n}\right]^{-1} \tag{4}$$

where K_e^n is the thermal conductivity for electrons embedded in a proportionally dense neutral gas. Following Banks (1966) and Chapman and Cowling (1952)

$$K_e^n = \frac{2}{3}\left(\frac{n_e}{N_n}\right) k \left[\frac{8\ k\ T_e}{\pi\ m_e}\right]^{\frac{1}{2}} \frac{1}{\overline{Q}_{dn}} \tag{5}$$

where Q_{dn} is the velocity averaged momentum transfer cross section for electrons passing through a neutral gas. That is,

$$\overline{Q}_{dn} = \left[\frac{m_e}{2\ k\ T_e}\right]^3 \int_o^\infty v_e^5\ q_D(v_e) \exp\left(-\frac{m_e\ v_e^2}{2\ k\ T_e}\right) dv_e \tag{6}$$

q_d = the velocity dependent momentum transfer cross section. This quantity is readily found from the published results of many experimenters (see McDaniel (1964) for a general reference).

N_n = the density of the n^{th} neutral species.

v_e = the electron velocity.

In the temperature range of interest, the thermal conductivity is given by

$$K_e = \frac{A\ T_e^{5/2}}{1 + B\ \frac{T_e^2}{n_e} \sum_{m=1}^{5} N_m Q_{dm}} \text{ (ergs cm}^{-1}\text{sec}^{-1}\ {}^{o}\text{K}^{-1}\text{)} \tag{7}$$

where

$$A = 1.23\times10^{-6}$$

$$B = 3.22\times10^{4}$$

$$Q_{d1} = 2.82\times10^{-17}T_e^{\frac{1}{2}} - 3.41\times10^{-21}T_e^{3/2} \quad cm^2$$

$$Q_{d2} = 2.24\times10^{-16} + 7.92\times10^{-18}T_e^{\frac{1}{2}} \quad cm^2$$

$$Q_{d3} = 3.4\times10^{-16} \quad cm^2$$

$$Q_{d4} = 5.6\times10^{-16} \quad cm^2$$

$$Q_{d5} = 5.47\times10^{-15} - 7.45\times10^{-19}\ T_e \quad cm^2$$

The subscripts 1, 2, 3, 4, 5 stand for the species N_2, O_2, O, He, and H respectively. This ordering of the species is adopted throughout the remainder of the discussion.

The rate of conversion of solar flux to thermal energy in the ambient electron gas, Q_e, is given by

$$Q_e = \sum_{i=1}^{5} N_i \sum_{\lambda} \epsilon_{i,\lambda}\ \phi_\lambda\ \sigma_{\lambda,i}^{(I)}\ \exp(-\tau_\lambda) \qquad (8)$$

$$\tau_\lambda = \sum_{i=1}^{5} \frac{\sigma_{i,\lambda}^{(A)}}{\cos\chi}\left[\frac{N_i\ k\ T_n}{m_i\ g} - C\right] \qquad (9)$$

where χ = the solar zenith angle

$\sigma_{i,\lambda}^{(I)}$ = the ionization cross section for species i and wavelength λ

$\sigma_{i,\lambda}^{(A)}$ = the corresponding absorption cross section

ϕ_λ = the solar flux in the range $d\lambda$ about λ

$\epsilon_{i,\lambda}$ = the energy conversion efficiency per electron-ion pair produced

g = the acceleration of gravity

C = a small constant

The values of the solar flux and cross sections are taken from Hinterreger et. al. (1965) in the wavelength range of 10-1027A. The energy conversion efficiency can be estimated from the available photon energy at each wavelength and the ionization potentials associated with each species. It is also necessary to consider the fraction of energy produced that is deposited locally in the electron gas by the photoelectrons. For the purposes of this study, an average value of 2 ev per electron-ion pair produced by photoionization has been found to be a suitable value. The effects of the detailed calculation to estimate $\epsilon_{i,\lambda}$ will be presented in a future paper. Hanson and Cohen (1968) have attempted to experimentally determine such an efficiency factor from radar backscatter data for T_e and N_e. The result of using such an efficiency is to shift the height of the maximum of both electron heat production and of the electron temperature upward in conformity with some of the observed data.

The rate at which electrons lose their thermal energy to the ion and neutral gases, L_e, is determined from the velocity dependent momentum transfer cross section [Desloge (1962)]. These cross sections, aside from the electron-ion coulomb cross section, are the result of laboratory measurements on nearly mono-energetic electrons passing through a background of the specified

neutral gas. The resulting velocity dependent cross sections are then averaged over a Maxwellian velocity distribution to obtain the energy loss from the passage of a hotter Maxwellian gas through a cooler one. Following Desloge (1962), the rate of energy loss from electrons to another species, s, is

$$L_{es}=4\pi n_e n_s \frac{m_e m_s}{(m_e+m_s)^2} \frac{(m_e m_s)^{5/2}(T_e-T_s)}{(2\pi k)^{3/2}(m_s T_e+m_e T_s)^{5/2}} \int_o^\infty v_r^5 q_o(v_r) e^{-\Omega v_r^2} dv_r \qquad (10)$$

where n, m, and T refer to the appropriate densities, masses, and temperatures, and where

v_r = the relative velocity between electrons and species, s

$$\Omega = [2k(\frac{T_e}{m_e} + \frac{T_s}{m_s})]^{-1}$$

The experimental values of $q_d(v_r)$ can be approximated by a power series of the form

$$q_D(v_r) = \sum_n A_n v_r^n + \sum_n \sigma_n \delta(v_r-v_{on}) \qquad (11)$$

The first term is used to fit the general trend of the data while the second can be used to account for important fluctuations. σ_n is the strength of such a fluctuation at $v_r = v_{on}$, and is determined by the requirement that the total cross section, q_t, in a velocity range (Δ v) be given by

$$q_t = \int_v^{v+\Delta v} \sum_n A_n v_r^n + \sum_n \sigma_n \delta(v_r-v_{on})]dv_r$$

The resulting form of the loss function is

$$L_{es} = \frac{4kn_e n_s}{\sqrt{\pi}} \frac{m_e m_s}{(m_e+m_s)^2}\left[2k\left(\frac{T_e}{m_e} + \frac{T_s}{m_s}\right)\right]^{\frac{1}{2}}(T_e-T_s)\left[\sum_n A_n \Omega^{-\frac{n}{2}} \Gamma\left(\frac{n+6}{2}\right)\right.$$

$$\left. +2 \sum_n \sigma_n \nu_{on}^{5/2} \exp(-\Omega\ \nu_{on})\right] \qquad (12)$$

For a multiconstituent gas the electron heat loss function is assumed to be given by

$$L_e = \Sigma\ L_{es} + L_{ei} \qquad (13)$$

Losses from electrons to ions via coulomb collisions are

$$L_{ei} = 4\sqrt{2\pi}\ \frac{n_e n_s e^4}{m_e\ m_i}\ k\ \frac{\ln\ \Lambda}{\left[k\left(\frac{T_e}{m_e} + \frac{T_i}{m_i}\right)\right]^{3/2}}(T_e-T_i) \qquad (14)$$

$$\ln\ \Lambda = 15.2$$

From equations (12, (13) and (14) the loss terms may be expressed in the following form

$$\sum_s L_{es} = 1.60\times10^{-12} n_e \{2.47\times10^{-18}[0](T_e-T_n)T_e^{\frac{1}{2}}$$

$$+1.71\times10^{-19}[N_2](1-2.1\times10^{-4}T_e)(T_e-T_n)T_e$$

$$+1.21\times10^{-18}[O_2](1+3.6\times10^{-2}T_e^{\frac{1}{2}})(T_e-T_n)T_e^{\frac{1}{2}}$$

$$+3.1\times10^{-14}[N_2](T_e-T_n)T_e^{-\frac{1}{2}}+10^{-13}[O_2](T_e-T_n)T_e^{-\frac{1}{2}}$$

$$+2.46\times10^{-17}[He]T_e^{\frac{1}{2}}(T_e-T_n)$$

$$+9.63\times10^{-16}[H](1-1.35\times10^{-4}T_e)(T_e-T_n)T_e^{\frac{1}{2}}\}\ (\text{ergs cm}^{-3}\text{sec}^{-1})$$

$$L_{ei} = 7.68\times10^{-19} n_e^2 (T_e-T_i)\ T_e^{-3/2}\ (\text{ergs cm}^{-3}\text{sec}^{-1})$$

ION TEMPERATURES

The ion temperatures are obtained for each ionic species by solving the appropriate heat conduction equation in a manner exactly analogous to that for T_e. The source of thermal energy is provided mainly by the hotter electrons via coulomb collisions, while the losses arise from collisions with the neutral gas. This means that at low altitudes the temperatures for each ionic specie are strongly coupled to the neutral gas temperature, and at high altitudes to the electron temperature. Equality of the ion temperature, T_i, at high altitudes with T_e is prevented by the relatively large ion thermal conductivity which enables heat energy to be conducted downwards and ultimately dissipated by the neutral gas. The ion thermal conductivity, K_i, based on the ion-ion interaction, has been given by Chapman (1952) and has the same temperature dependence as K_e.

The ion temperature equation has the form

$$\frac{\partial T_i}{\partial t} - \frac{\sin^2 I}{n_i k C_v} \frac{\partial}{\partial z} \left[K_i \frac{\partial T_i}{\partial z}\right] = \frac{P_i - L_i}{n_i k C_v} \qquad (15)$$

when the effects of motion are neglected. Since ionic composition is not being discussed in this work, only the major ion, O^+, is considered. However, it should be recognized that the usually minor ions, H^+ and He^+, can be heated more efficiently than O^+, and so can play an important role whenever their densities are sufficiently close to the O^+ density. For O^+, the following

expressions give K_i, P_i and L_i.

$$K_i = 9.51\text{x}10^{-20} T_i^{5/2}/m_i^{\frac{1}{2}} \text{ (ergs cm}^{-1}\text{sec}^{-1}\ {}^{o}\text{K}^{-1})$$

$$P_i = L_{ei} \text{ (ergs cm}^{-3}\text{sec}^{-1})$$

$$L_i = n_i\{1.06\text{x}10^{-25}[N_2]+9.3\text{x}10^{-26}[O_2]+3.36\text{x}10^{-27}[O](T_i+T_n)^{\frac{1}{2}}$$
$$+4.49\text{x}10^{-26}[He]+5.3\text{x}10^{-26}[H]\}(T_i-T_n) \text{ (ergs cm}^{-3}\text{sec}^{-1})$$

NEUTRAL TEMPERATURE

The heat conduction equation for the neutral temperature, T_n, is based directly on that given by Harris and Priester (1962), but with three modifications. Since only the steady state results are of interest, the expansion velocity term is not included as it depends directly on the time rate of change of the neutral temperature. The heat input from the electron and ion gases are added to the heat input from the direct absorption of solar energy. This additional energy amounts to about 15-20% of the total heat input. Finally, a representative solar spectrum and corresponding ionization and absorption cross sections, as given by Hinterreger et. al. (1965), are used instead of the average values. Use of average values leads to a substantial error and can have a considerable effect on the distribution of thermal energy in the E and lower F regions of the ionosphere.

The neutral gas temperature equation is given by

$$\frac{\partial T_n}{\partial t} - \frac{1}{kN_T}\frac{\partial}{\partial z}\left[K_n \frac{\partial T_n}{\partial z}\right] = \frac{Q_n - L_n}{kN_T} + \frac{L_{es}+L_i}{kN_T} \qquad (16)$$

where

$$K_n = \frac{\sum_n A_m N_m}{\sum_m N_m} T_n^{\frac{1}{2}} \text{ ergs cm}^{-1}\text{sec}^{-1}\ {}^{o}\text{K}^{-1}$$

is the density weighted approximation to the thermal conductivity of a multicomponent neutral gas

A_1=180 A_4=360

A_2=180 A_5=2100

A_3=180 $N_T=\sum_m N_m c_{vm}$

c_{vm} is the specific heat at constant volume for the m^{th} neutral constituent (c_{vm}=3/2 for atomic species and 5/2 for diatomic species)

The energy input to the neutral gas from super elastic collisional conversion of the absorbed solar radiation is given by

$$Q_n = \sum_{m=1}^{5} Nm \sum_{\lambda} \beta_{m\lambda} I_{\lambda} \sigma_{\lambda m}^{(A)} \exp(-\tau_{\lambda})$$

where $\beta_{m\lambda}$= the fraction of the absorbed energy that is transformed into thermal energy. In this paper a constant value of 0.2 is used so that realistic values of temperature could be

obtained for the range of solar flux considered in this paper. I_λ is the intensity of the solar radiation in the wavelength range $\Delta\lambda$ about λ. Finally, the loss term, L_n, arising from the infrared radiation emitted by thermally excited atomic oxygen, is given by [Bates (1951), Lazerev (1963)].

$$L_n = [O] \frac{1.6\times10^{-18}\exp(-228/T_n)}{1+0.6\exp(-228/T_n)+0.2\exp(-325.3/T_n)} \text{ (ergs cm}^{-3}\text{sec}^{-1}\text{)} \tag{17}$$

The distribution of the neutral constituents with altitude, z, is assumed to follow the hydrostatic distribution for $z > z_L$.

$$N_m(z) = \frac{N_m(z_L)T_n(z_L)}{T_n(z)} \exp\left\{-\int_{z_L}^{z} \frac{m_m g(z')}{k\, T_n(z')}\, dz'\right\} \tag{18}$$

where the boundary values $N_m(z_L)$ for the species $[N_2]$, $[O_2]$, and $[O]$ are important input parameters whose variations are discussed in a later section. z_L and z_u are the lower and upper boundary altitudes, respectively. The remaining neutral species, He and H, are also described by the above equation. However, no significance can be attached to the values computed at low altitudes since it is only above about 400 km to 500 km that hydrostatic equilibrium is an appropriate approximation for He and H. Below this altitude they have little effect on the model because of their relatively small density.

ELECTRON DENSITY

Once the various temperatures are specified by the preceding equations, the electron density can be obtained by solving the continuity equation together with the momentum equation. As with the ion temperatures, if the ionospheric composition is of interest, a separate continuity equation must be solved for each species. This involves specifying the expressions for the diffusion velocity and all important chemical and ionization processes. The solution of the resulting system of equations will be discussed in another paper. Since only the electron density is of interest here, a form of the continuity equation proposed by Shimizaki (1965) is used. This form accounts for the presence of the minor ions N_2^+, O_2^+, and NO^+ in the E and lower F regions through modifications of the effective rate of photoionization and chemical recombination. The specific form used is

$$\frac{\partial [O^+]}{\partial t} + \nabla \cdot ([O^+]\vec{v}_{O+}) = \sum_{i=1}^{3} A_i Q_i - L n_e^2 \qquad (19)$$

where

$$L = \frac{\lambda_1 [O_2] + \lambda_2 [N_2]}{n_e + \frac{\lambda 1}{\alpha_1}[O_2] + \frac{\lambda 2}{\alpha_2}[N_2]}$$

$$\delta = \frac{n_e + (\frac{\lambda_3}{\alpha_2} + \frac{\lambda_5}{L}[O] + (\frac{\lambda_4}{\alpha_2} + \frac{\lambda_6}{\alpha_1})[O_2]}{n_e + (\frac{\lambda_3 + \lambda_5}{\alpha_3})[O] + (\frac{\lambda_4 + \lambda_6}{\alpha_3})[O_2]},$$

and $A_1 = \frac{\delta L}{\alpha_3}$ $A_2 = \frac{L}{\alpha_1}$ $A_3 = 1$.

The numerical values of the reaction rate coefficients are adopted from Whitten and Poppoff (1964)Ferguson (1968), Warneck, (1966), and are given in units of $cm^3 sec^{-1}$.

$\alpha_1 = 7x10^{-5} T_n^{-1}$ $\lambda_3 = 2.5x10^{-10}$

$\alpha_2 = 1.5x10^{-3} T_n^{-3/2}$ $\lambda_4 = 2x10^{-13}$

$\alpha_3 = 5x10^{-5} T_n^{-3/4}$ $\lambda_5 = 2x10^{-12}$

$\lambda_1 = 2x10^{-11}$ $\lambda_6 = 2x10^{-10}$

$\lambda_2 = 2x10^{-12}$

These values were selected as representative from among the many choices in the literature. The variations between the various choices produce changes of little consequence for the F region electrons and 0^+ ions.

Equation (19) has been obtained from Shimizaki's equation (13) (Shimizaki, 1965) by making several approximations. (From the numerical values of the rate coefficients it is possible to show that L/α_1, L/α_2, and $\delta L/\alpha_3$ become very small above about 200 km. Below 200 km the divergence terms, $\nabla.([O_2^+]v_{O_2^+})$, $\nabla.([N_2^+]v_{N_2^+})$, and $\nabla.([NO^+]v_{NO^+})$ are almost entirely negligible. This means that the terms multiplied by L/α_1, L/α_2, and $\delta L/\alpha_3$ need not be considered for steady state solutions.)

Equation (19) does not include He^+ and H^+. For the midday conditions discussed in this paper, the He^+ and H^+ densities are sufficiently less than the O^+ density so that both the approximation $[O^+] \cong n_e$ and the neglect of He^+ and H^+ are applicable throughout the height range of interest. Of course, this cannot be done when the diurnal variation is discussed since the influence of H^+ is usually dominant in the F region at night.

The divergence term in equation (19) can be evaluated from the usual momentum equations [Burgers (1960), Chandra (1964)].

$$m_e n_e \left(\frac{\partial \vec{v}_e}{\partial t} + \vec{v}_e \cdot \nabla \vec{v}_e\right) = -\nabla p_e + m_e n_e \vec{g} - e n_e \left(\vec{E} + \frac{1}{c} \vec{v}_e x B\right) - \sum_s K_{es} (\vec{v}_e - \vec{v}_s) \tag{20}$$

$$m_{O^+}[O^+]\left(\frac{\partial \vec{v}_{O^+}}{\partial t} + \vec{v}_{O^+} \cdot \nabla \vec{v}_{O^+}\right) = -\nabla p_{O^+} + m_{O^+}[O^+]\vec{g} + e[O^+]\left(\vec{E} + \frac{\vec{v}_{O^+}}{c} x\vec{B}\right) - \sum_s K_{O^+ s} (\vec{v}_{O^+} - \vec{v}_s) \tag{21}$$

$$m_n N_n \left(\frac{\partial v_n}{\partial t} + \vec{v}_n \cdot \nabla \vec{v}_n\right) = -\nabla p_n + m_n N_n \vec{g} - \sum_s K_{ns} (\vec{v}_n - \vec{v}_s) \tag{22}$$

where

$$P_j = N_j k T_j \tag{23}$$

g = the acceleration of gravity

e = the electronic charge

B = the earth's magnetic field in gauss

$K_{ij} = K_{ji} = n_i \mu_{ij} \nu_{ij}$

$\mu_{ij} = m_i m_j/(m_i+m_j)$

ν_{ij} = the momentum transfer collision frequency (see appendix for numerical evaluation).

It is now assumed that $\vec{v}.\nabla\vec{v}$ can be neglected and that the neutral gas velocity $\vec{v}_n$ can be treated as an unknown parameter of the problem combined with the hydrostatic approximation for the neutral gas distribution with altitude, $\nabla p_n \cong N_h m_h \vec{g}$. Finally, for the case where $v_n \cong 0$ and $\nu_{ij}/(eB/m_j) \ll 1$ and making use of the continuity equation $\nabla.(n_e\vec{v}_e - [O^+]\vec{v}_{O^+}) \cong 0$, equation (22) for a horizontally stratified ionosphere may be approximated in the following form Chandra (1965)

$$\frac{\partial n_e}{\partial t} - \sin^2 I \frac{\partial}{\partial z}\left\{\frac{\frac{\partial}{\partial z}[n_e k(T_e+T_i)]+n_e(m_e+m_i)g}{\sum_{s=1}^{5}[\mu_{O^+s}\nu_{O^+s}+\mu_{es}\nu_{es}]}\right\} = \sum_{m=1}^{3} A_m Q_m - L\, n_e^2 \qquad (24)$$

Equation (24) along with equations (2), (15), (16), and (18) can be solved with the appropriate boundary conditions to give the profiles for N, n_e, T_e, T_i, and T_n in the height range between z_L and z_u.

NUMERICAL METHOD

The system of equations presented in the preceding sections is clearly not suited for finding an analytical solution under realistic conditions. Therefore, a particular numerical approach was adopted from among several possibilities that seemed feasible for this problem. Direct solution of the steady state equations was abandoned in favor of methods where the time derivative in each equation asymptotically approaches zero as time increases. The direct use of the steady state equations is very convenient when solving one of the equations of the system by itself. Rishbeth and Barron (1960) demonstrated in an ionospheric application how the difficulties in applying the boundary conditions can be overcome for the steady state equations by a trial and error procedure. However, when the method is applied to a system of coupled equations the result is far too cumbersome to be practical. The use of the time dependent equations to obtain an asymptotic approach to stationary conditions permits a straightforward numerical solution and leads naturally to the solution of the same equations for their diurnal behavior.

All the equations are of the form

$$\frac{\partial \Psi_i}{\partial t} + A_i(z,t;\Psi_i,\frac{\partial \Psi_i}{\partial z};\Psi_j)\frac{\partial^2 \Psi_i}{\partial z^2} + B_i(z,t;\Psi_i;\Psi_j)\frac{\partial \Psi_i}{\partial t} + c(z,t;\Psi_i;\Psi_j)=0$$

where i and j are subscripts referring to the several dependent variables.

As far as the authors know, there is no theoretically described method for solving such a system of equations. In the absence of such methods there are two basic practical approaches to be taken. First, one can linearize the equations so as to apply the well known theorems of linear and quasi-linear systems, [Ames (1965)]. Second, one can adopt a partial linearization and iteration technique which is applied repeatedly at each time step until the nonlinear equations are solved to some desired degree of accuracy. For example, the coefficients A, B, and C are calculated from an arbitrary set of initial values for the Ψ_i. The solution is then obtained for the next time, $0 + \Delta t$, by the implicit difference technique and iteration to obtain $\Psi_i(0+\Delta t)$. Next, A, B, and C are recalculated using the new values, and solutions are obtained for $\Psi_i(0+2\Delta t)$. If the repeated process is non-divergent, stable, and yields a set of values, $\Psi_i(t)$, that simultaneously satisfy the original system of equations and their boundary conditions to an accuracy within the truncation error caused by numerical differentiation, then a solution has been obtained. For the equations applied to the ionosphere, a great deal of care must be taken so that numerical significance is not lost when evaluating the space derivatives. This is especially true of the second derivatives in the height region from 100 to 200 km.

The form of the boundary conditions applied are

$$\Psi_i(z_L,t) = f_i(t)$$

$$\left.\frac{\partial \Psi_i}{\partial z}\right|_{z_u,t} = \phi_i(t)$$

where

$$\Psi_i = (T_e, T_n, T_i, n_e)$$

$$z_L = 100 \text{ km}$$

$$z_u = 1000 \text{ km}$$

$f_i(t)$ and $\phi_i(t)$ are known specified functions of time.

Representative boundary conditions for the individual equations are shown in Table 1.

TABLE 1

Dependent Variable	Upper BC	Lower BC
n_e	velocity specified	production=loss
T_e	$\frac{\partial T_e}{\partial z} = 0.5^{\circ}$/km	$T_e = 226^{\circ}$K
T_i	$\frac{\partial T_i}{\partial z} = 0.5^{\circ}$/km	$T_i = 225.5^{\circ}$K
T_n	$\frac{\partial T_n}{\partial z} = 0.0^{\circ}$/km	$T_n = 225^{\circ}$K

The choice of these values is discussed in detail in a later section.

DISCUSSION OF THE SOLUTIONS

In this section a few selected cases are presented to show the general characteristics of the simultaneous solutions of the equations for T_e, T_i, T_n, and n_e. All the cases presented are for conditions of latitude and dip prevailing at Wallops Island, Virginia (latitude of 37° and dip of 70°) or at Arecibo, Puerto Rico (latitude 18° and dip 50°), and for a range of solar flux corresponding to high and low activity (noontime conditions with a declination computed for March 2).

To facilitate comparison between the various results, only the solar flux entering the ionosphere and the density of the neutral constituents at 100 km are varied as parameters of the problem. This means that the neutral atmospheric composition and corresponding heat and ionization input functions (Q_e, Q_L, Q_n, and P_e) are determined in a self-consistent manner with T_e, T_i, T_n, and n_e and their boundary conditions. There are other free parameters that can be varied (reaction rates, collision cross sections, ionization cross sections, etc.), but to avoid an unnecessarily complex discussion they were held constant at values given by recent experimental results. Reference values for the N_2, O_2, and O densities at 100 km were extrapolated from the measured values obtained during the Geoprobe* rocket flight of March 2, 1966. [Hall et al 1967] This flight made simultaneous measurements of the

*Preliminary data presented at the A.G.U. meeting in Washington, D. C. (April 1968) by Brace, L., Findlay, J. A., and Mayr, H. G. (paper Ga89) and by Pelz, D. T. and Newton, G. P. (paper GA86).

neutral composition, neutral temperature, ion composition, and electron density. The boundary values for He and H at 100 km are given in Table 2. The gradient of 0.5^{o}/km at an altitude of 1000 km for T_e and T_i was selected as being representative of the available data which ranges from 0^{o}/km to 2^{o}/km. The boundary condition for the electron density was obtained by specifying the electron velocity as some reasonable value. It was found that velocities less than 100 meters per second had no significant effect on the solutions, while those in excess of this value caused considerable distortions from measured profiles. In addition, velocities of about 100 meters per second are an upper limit since they correspond to a flux of about $10^{8}cm^{-2}sec^{-1}$. A flux of this size cannot be maintained for an extended period of time either into or out from the upper ionosphere[Geisler (1967)]. The lower boundary at 100 km for the electron density was selected so as to satisfy the conditions of chemical equilibrium under all circumstances. If a different value was tried at 100 km, the solution at 110 km automatically assumed a value such that chemical equilibrium was reestablished. Significant deviations from chemical equilibrium began to appear at 120 km and higher. Finally, the values of T_e, T_i, and T_n were selected as 226^{o}, 225.5^{o}, and 225^{o}K at 100 km, respectively. It was found that the solutions are relatively insensitive to this choice. There are three final parameters which help determine the character

of the solutions. These are the neutral and charged particle heating efficiencies and the ionization efficiency. The first is an estimate of the fraction of solar energy absorbed by the neutral gas that becomes transformed into thermal (kinetic) energy by superelastic collisions involving neutral particles in an excited state. The second is an estimate of the number of electron-volts per ion-electron pair created that is ultimately deposited in the ambient electron gas as kinetic energy. This process involves the removal of energy from high velocity photoelectrons and their associated secondary impact ionization electrons. Several authors have made detailed calculations for this process [Dalgarno et. al. (1963), Mariani (1964)]. Finally, the ionization efficiency accounts for the number of electrons produced per incident photon both by primary and secondary ionization process. The values adopted here are 20%, 2 ev/electron-ion pair, and 1.5 electron-ion pairs per primary electron ion pair produced. Actually, these quantities should be determined as self-consistent height dependent quantities along with the other unknowns upon which they depend. The uncertainty in the theoretical expressions for the efficiencies is too great to warrant the added complexity.

Since the values measured by the Geoprobe rocket are used as a reference in obtaining the lower neutral atmospheric boundary conditions, a comparison is presented between the theoretical and experimental profiles. In Figure 2 the upper

half corresponds to smoothed curves drawn through the data points obtained from the Geoprobe rocket. The T_n values are determined from the measured molecular nitrogen densities (the dashed portion of the curve is an extrapolation based on the assumed near isothermality at high altitudes), the T_e profile was taken from the cylindrical probe data, and the electron density from the propagation experiment carried on board the rocket. The lower half of the figure represents the corresponding theoretical model. As mentioned before, a fixed set of upper boundary conditions was used with no attempt to match the measured gradient from the Geoprobe experiment of 2^{o}/km. In spite of this, the agreement is quite reasonable over the entire altitude range for both T_n and n_e. Much closer agreement can be obtained when the fully time dependent equations are solved. The time dependent solutions admit the presence of large thermal gradients at high altitudes for limited portions of the day as long as the downward heat flow during the day does not exceed the available energy from the protonosphere. In the steady state models presented here the use of 2^{o}/km as a boundary condition on T_e at 1000 km leads to unrealistic results. The free parameters used to obtain the theoretical profiles are given in Table 2. The solar flux listed as 0.95*HF is scaled to be 95% of the flux given by Hinterreger, et. al. (1965). The adjustment of the solar flux is done so that the neutral exospheric temperature

TABLE 2

Latitude = 37^{o} $\chi = 39^{o}$ (solar zenith angle)

Dip = 70^{o} Day = March 2

Solar Flux = 0.95*HF

Neutral Density at 100 km (cm^{-3})

$[N_2]=4.65x10^{-12}$ $[O_2]=1.25x10^{12}$ $[O]=6.75x10^{11}$

$[He]=2.50x10^{8}$ $[H]=1.00x10^{8}$

approximately corresponds to the measured values. However, the resulting solutions showed that the adjusted solar activity necessary to give agreement with experimental results is close to the observed solar activity for March 2, 1966. It was also required that the range of solar flux used be approximately a factor of 2 in order to change the exospheric neutral temperature from solar minimum conditons (about 700^{o}) to solar maximum conditions (about 1800^{o}). The necessary flux was obtained by multiplying the Hinterreger flux (HF) (corresponding to a 10.7 cm flux of about S=85) by a series of factors ranging from 0.85 to 1.75.

Before discussing the effects of the varying solar flux, it is of interest to see how the neutral composition effects the solutions. In Figure 3 the upper half shows the results obtained by varying the molecular nitrogen density at 100 km for two values of the solar flux, 1.15*HF and 1.75*HF. The

main effect of this variation is to increase the neutral temperature and thereby the absolute concentration of atomic oxygen. Since this also implies an increase in optical depth and the rate of ionization (and thus heat input), it is consistent that the height of the electron temperature maximum rises as does the height of the maximum of electron density. An important change shows up in the gradients of T_e and T_i (T_i not shown). These gradients control the shape of the electron density profile to a large degree. Of course, the profiles obtained for n_e at high solar flux cannot be realistic because of the high altitude of the F2 peak[Rishbeth (1968)]. It is shown later that varying the atomic oxygen density at the lower boundary in proportion to the solar flux is sufficient to remove the difficulty. The lower boundary value used for atomic oxygen in figure 3 is $6.75 \times 10^{11} cm^{-3}$. The results and conclusions for varying the molecular oxygen density, as shown in the lower half of Figure 3, are analogous to those for molecular nitrogen.

It should be pointed out that the effects of varying atomic oxygen depend on the way the variation is introduced. In the above case, the variation was caused by an increase in T_n brought on by another source. However, if only the value of atomic oxygen at 100 km is increased, then a different sequence of events takes place. Specifically, the neutral

temperature decreases since the neutral heat loss function is proportional to the atomic oxygen density and the increased heat input from the electrons and ions is insufficient to make up the difference unless the increase in atomic oxygen density is small. In turn, the decrease in T_n causes a depression of the peak heights in T_e and n_e, a decrease in n_e above the F2 maximum, and an increase below the maximum. Thus, more than any other neutral constituent, atomic oxygen plays the basic role in determining the characteristics of the E and F regions. This is particularly so, since it is also the neutral constituent that is most responsive to changes in the solar flux. Thus, variation of atomic oxygen with solar flux must play an important role in the F region behavior. Such effects should also be seen if there are other energy inputs into the ionosphere that significantly change the dissociation rates or raise the turbopause level (by expansion of the mesosphere due to heating). For example, the effects seen long after the onset of a magnetic storm may arise by the inverse of the above processes. This effect is discussed in the accompanying paper.

The solar cycle variation of T_e, T_i, T_n, and n_e at two latitudes was investigated for two sets of boundary conditions. The first set has the atomic oxygen density independent of the solar flux, while the second set assumes an empirical linear relationship between the two. Figures 4 to 9 show the effects of the solar flux variation (in steps of 0.85, 1.15, 1.45, and

1.75*HF) for three fixed values of the atomic oxygen density at 100 km, 5.39×10^{11}, 6.75×10^{11}, and 8.11×10^{11} cm^{-3}. The first three of these figures are for a latitude and dip corresponding to Wallops Island, Virginia and the second three are for Arecibo, Puerto Rico. Some general features can be noted by direct comparison among the figures. First, in all cases the height of the F2 maximum increases with increasing solar flux, as does the neutral temperature, the total electron content, the total electron heat content ($1.5 \int n_e k T_e dz$), the total ion and neutral heat contents, the height and magnitude of the maximum of T_e, and the magnitude of T_i. These changes are accompanied by increases in the absolute concentrations of the neutral constituents at a fixed altitude, and by changes in the ratios of their densities. However, as can be seen from Figures 4 to 6 there are two distinct forms for the T_e profile. The first form shows a peak in the vicinity of 200 km followed by a steep negative temperature gradient, while the second form is monotonically increasing except perhaps for a small region near 200 km. Of course, there exists a smooth transition between one form and the other, but over a moderately narrow range of the free parameters. As is shown, a change from 0.85 to 1.15*HF is sufficient to complete the transformation. The T_e profile labeled 1.05 in Figure 5 is included to show the smooth transition. The ion temperature associated with

the first form of T_e increases smoothly with solar flux in the exosphere following the trends of T_e. At lower altitudes, below about 200 km, the ion temperature closely approaches T_n in behavior and magnitude. However, as is shown in figures 4 to 6, whenever the second form of T_e is encountered the behavior of T_i with solar flux is inverted until the solar flux is increased to where the first form of T_e appears. The effect of the second form of T_e on the electron density profile is to strongly change the slope above the F2 maximum. The structure in the n_e profiles below the F2 maximum is caused by the gradients in the temperature profiles and by the various reaction rates contributing to the net electron production rate. The structure shown is suggestive of typically observed electron density profiles, but this comparison cannot be pursued until the detailed ion composition corresponding to this structure is also discussed. Finally, the effect of latitude shown in the two sets of figures is to cause the heights of the maximums of T_e and n_e to increase. That is, as the latitude decreases the solar zenith angle decreases and the dip angle decreases, both of which have the effect of raising the heights of the temperature and density maximum.

As mentioned before, the unrealistically high altitudes of the F2 maximum for high solar flux values can be overcome by increasing the atomic oxygen content in proportion to the

solar flux. Such increases are consistent with those proposed by Shimizaki (1967) in a recent paper discussing this aspect of the neutral atmosphere. That is, the photodissociation rate of O_2, eddy mixing, and the reactions into which atomic oxygen enters are such that the variation with solar flux is reasonable. The results of this procedure are shown in Figures 10 and 11. Thus, it is possible to obtain reasonable F2 maximum heights while still enabling the other parameters, T_e, T_i, T_n, and n_e, to change in a way appropriate to the solar flux. Because of the neutral temperature's dependence on the atomic oxygen density for heat loss, the resulting T_n values are lower in general for increased atomic oxygen density. The trend is not absolutely clear cut because of the increased ionization and thus the increased heat transfer from the electron and ion gases to the neutral gas. Even though the trends shown are consistent with observations, a detailed comparison is not made here since the atomic oxygen variation was carried out on a strictly empirical basis. The inclusion of the neutral chemistry and the associated reaction rates should make quantitative comparison possible.

CONCLUSION

Theoretical profiles for T_e, T_i, T_n, and n_e have been obtained by numerical solutions of the coupled partial differential equations describing the E and F regions of the ionospheric

plasma. The results obtained show the complex interrelationship between the several dependent variables and thus the necessity of obtaining simultaneous self-consistent solutions. In particular, the following conditions can be enumerated as the result of the present investigation.

1. The neutral temperature of the upper atmosphere is strongly dependent on the solar flux and on the neutral composition at the turbopause level. The temperature increases with increases in the O_2 density or N_2 density but decreases when the density of atomic oxygen is increased.

2. The electron density above the F2 peak increases with solar flux as does h_{max}, n_{max}, and the total electron content. In addition, the electron density in the region of the F2 maximum increases with T_n unless the increase in T_n is the result of a decrease in the atomic oxygen concentration at low altitudes.

3. The composition at the lower boundary cannot be assumed constant throughout the solar cycle since it leads to unrealistic values of the F region parameters for sunspot maximum conditions. This difficulty was overcome by assuming an increase in the atomic oxygen density at the reference altitude proportional to the solar flux. The need for this variation shows the necessity for constructing a more complete model incorporating the neutral chemistry and mixing effect that are so important near the turbopause level.

4. The electron temperature does not show a definite pattern of variation of the same regularity as the neutral temperature or the electron density. However, the integrated heat content, $c_v \int n_e k T_e dz$, increases with solar flux. The electron temperature is characterized by two types of profiles. The first shows a peak in the vicinity of 200 km while the second type is monotonically increasing almost everywhere. The smooth but rapid transition between the two types of profiles when conditions are changed occurs during low solar activity. The transition is governed mainly by the value of T_n, going from a monotonically increasing profile to a peaked profile with a considerably reduced exospheric electron temperature. For high solar flux, T_e varies in proportion to the solar flux at all altitudes above the peak.

5. The ion temperature behaves quite regularly unless the electron temperature undergoes a transition from one form to another as conditions are changed. At low altitudes the ion temperature closely follows the neutral temperature. However, above approximately 200 km, T_i starts to follow the trends in the electron temperature and frequently approaches T_e at high altitudes.

ADDENDUM

At the time of the completion of this work, Dalgarno and Degges (Planetary and Space Science, 16, 125, 1968) published a paper showing that the dominant cooling mechanism for the electron gas results from the fine structure excitation of atomic oxygen. We have since included this heat loss in our calculations. A typical example of the changes resulting from the additional electron cooling is shown in the following table. The conditions used correspond to the case HF=1.15 in Figure 5.

Ionospheric Parameters	Including Atomic Oxygen Fine Structure Cooling	Without Atomic Oxygen Fine Structure Cooling
T_e (1000 km) ^oK	1750	1804
T_e (500 km) ^oK	1349	1416
T_e (max) ^oK	1195	2274
h ($T_e$max) km	190	180
T_N (1000 km) ^oK	859	859
T_i (1000 km) ^oK	1413	1530
n_e (1000 km) cm^{-3}	3.26×10^3	3.98×10^3
n_e (500 km) cm^{-3}	6.47×10^4	7.06×10^4
n_e (max) cm^{-3}	7.44×10^5	6.48×10^5
h ($n_e$max) km	260	260

As can be seen from the table, the main effect of this

cooling mechanism is to decrease T_e in the lower altitudes while leaving all the other parameters substantially unchanged. The main conslusions of this paper and the accompanying paper ("F-Region Ionization and Heating During Magnetic Storms") are not altered even though the electron temperature changes are considerable. The detailed implications of the atomic oxygen fine structure cooling of the electron gas will be discussed in a future paper.

ACKNOWLEDGMENT

The authors wish to thank S. J. Bauer, L. H. Brace, G. P. Newton, and C. A. Reber for providing the preliminary Geoprobe rocket data, and Mr. G. Miller for helping with the difficult computer programming.

BIBLIOGRAPHY

Ames, W. F., Nonlinear Partial Differential Equations in Engineering, Academic Press, (1965).

Banks, P. M., J. Geophys. Res., 72, 3365-3385 (1967).

Banks, P. M., Planet. and Space Sci., 14, 1085-1103 (1966a).
Banks, P. M., Planet. and Space Sci., 14, 1105-1122 (1966b).
Banks, P. M., Annals de Geophysique, 22, 577-587 (1966).

Bates, D. R., proc. Roy. Soc., London Section B64, 805-821 (1951).

Burgers, J., Symposium of Plasma Dynamics, 119-181, Addison Wesley (1960).

Chandra, S., J. Atmos. Terrestrial Phys., 26, 113-132 (1964).

Chandra, S., J. Atmos. Terrestrial Phys., 27, 1159-1162 (1965).

Chapman, S. and Cowling, T. G., The Mathematical Theory of Non-Uniform Gases, Cambridge (1952).

Dalgarno, A., McElroy, M., Moffett, R., Planet. Space Sci., 11, 463-484 (1963).

Dalgarno, A., McElroy, M., Walker, J., Planet. Space Sci., 15, 331-345 (1967).

Desloge, E. A., Phys. of Fluids, 5, 1223-1225 (1962).

Evans, J. V., Presented at the Int. Union Symp. Solar Terrestrial Physics, Belgrade (1966).

Ferguson, E. E., Review of Geophysics, 5, 305-327 (1968).

Geisler, J. E. and Bowhill, S. A., J. Atmos. Terrestrial Phys., 27, 1119-1146 (1965).

Geisler, J. E., J. Geophys. Res., 72, 81-85 (1967).

Hall, L. A., Chagnon, C. W., and Hinteregger, H. E., J. Geophys. Res., 72, 3425-3427 (1967).

Hanson, W. and Cohen, R., J. Geophys. Res., 73, 831-840 (1968).

Harris, I. and Priester, W., J. of Atmos. Sci., 19, 286-301 (1962).

Hinteregger, H., Hall, L., and Schmidtke, G., Space Research V, 1175-1190 (1965).

Lazarev, V. I., Geomagnetism i Aeronomiya, 3, 842-849 (1963)(NASA Technical Translation No. ST-AT-10094).

McDaniel, E., Collision Phenomenon in Ionized Gases, John Wiley & Sons (1964).

Mariani, F., J. Geophys. Res., 69, 556-560 (1964).

Nicolet, M., Planet. Space Sci., 5, 1-32 (1961).

Polyzkov, V. M., Geomagnetism i Aeronomiya, 6, 269-277 (1966).

Rishbeth, H., Rev. of Geophysics, 6, 33-72 (1968).

Rishbeth, H. and Barron, D., J. Atmos. Terrestrial Physics, 18, 234-252 (1960).

Shimazaki, T., J. Atmos. Terrestrial Physics, 27, 593-604 (1965).

Shimazaki, T., J. Atmos. Terrestrial Physics, 29, 273-747 (1967).

Spitzer, L., Physics of Fully Ionized Gases, Interscience (1965).

Spitzer, L., and Harm, R., Phys. Rev., 89, 977-981 (1953).

Warneck, P., Ion-Molecule Reaction Rates in an Oxygen-Nitrogen Atmosphere, GCA Technical Report No. 66-13-N (July 1966).

Whitten, R. C. and Poppoff, I. G., J. Atmos. Sci., 21, 117 (1964).

Yonezawa, T., Space Sci. Rev., 5, 3-56 (1966).

APPENDIX

The following are a list of effective collision frequencies for momentum transfer, ν_{ij}, taken from the equation for momentum transfer between two interpenetrating Maxwellian gases of possibly different temperatures and masses. The defining equation is

$$\nu_{ij} = \frac{8}{3\sqrt{\pi}}\, n_j \Omega_{ij}^{\frac{5}{2}} \int_0^\infty v_r^5 q_{oij}(v_r) \exp(-\Omega_{ij} v_r^2)\, dv_r$$

From this equation and the experimentally obtained velocity dependent momentum transfer cross sections, q_{dij}, numerical values of ν_{ij} can be obtained (Banks, 1966).

For electron-neutral collisions,

$$\nu_{e1}(e \rightarrow N_2) \cong 2.33 \times 10^{-11} [N_2] \{1 - 1.21 \times 10^{-4} T_e\} T_e$$

$$\nu_{e2}(e \rightarrow O_2) \cong 1.82 \times 10^{-10} [O_2] \{1 + 3.6 \times 10^{-2} T_e^{\frac{1}{2}}\} T_e^{\frac{1}{2}}$$

$$\nu_{e3}(e \rightarrow O) \cong 2.8 \times 10^{-10} [O] \{T_e^{\frac{1}{2}}\}$$

$$\nu_{e4}(e \rightarrow He) \cong 4.6 \times 10^{-10} [He] T_e^{\frac{1}{2}}$$

$$\nu_{e5}(e \rightarrow H) \cong 4.5 \times 10^{-9} [H] \{1 - 1.35 \times 10^{-4} T_e\} T_e^{\frac{1}{2}}$$

For ion-neutral collisions,

$$\nu_{3n}(O^+ \rightarrow \text{neutrals}) = 5.181 \times 10^{-11} [O] (T_i + T_n)^{\frac{1}{2}} (1 - 0.064 \ln(T_i + T_n))^2 + 1.798 \times 10^{-9} \sum_{\substack{s \\ s \neq 3}} N_s (\alpha_s / \mu_{3s})^{\frac{1}{2}}$$

where the polarizabilities, α (in units of cm^3) are given by

$$\alpha_1=1.76\text{x}10^{-24} \qquad \alpha_4=2.10\text{x}10^{-25}$$

$$\alpha_2=1.60\text{x}10^{-24} \qquad \alpha_5=6.70\text{x}10^{-25}$$

$$\alpha_3=8.90\text{x}10^{-25}$$

LIST OF FIGURES AND CAPTIONS

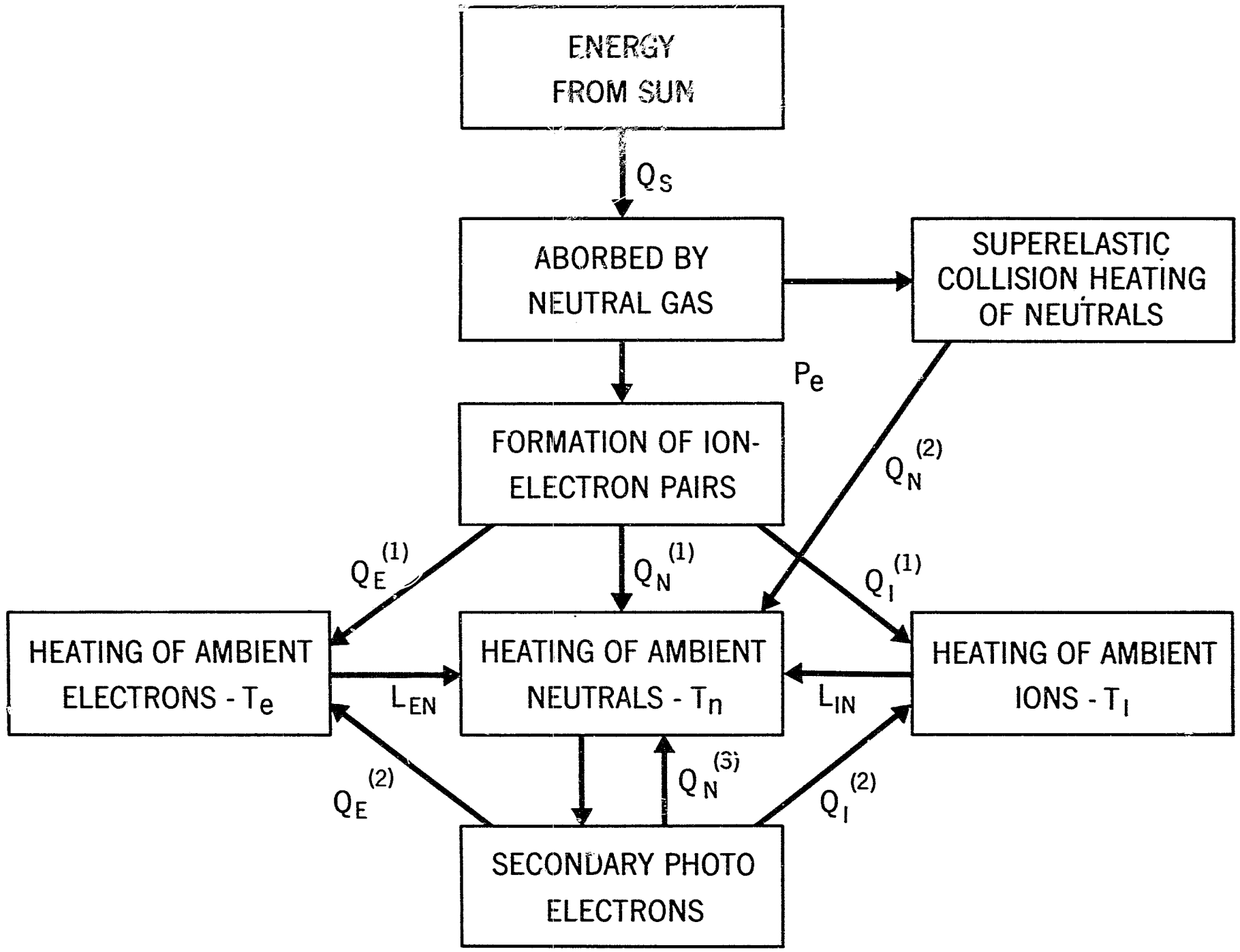

ENERGY SOURCE DIAGRAM

Figure 1.

COMPARISON WITH GEOPROBE DATA

LAT. = 37 DIP = 70° HF* = 0.95

χ = 39° DAY = MARCH 2

BC = 4.65^{12}, 1.25^{12}, 6.75^{11}, 2.50^{8}, 1.00^{5}

$[N_2]$ $[O_2]$ $[O]$ $[He]$ $[H]$

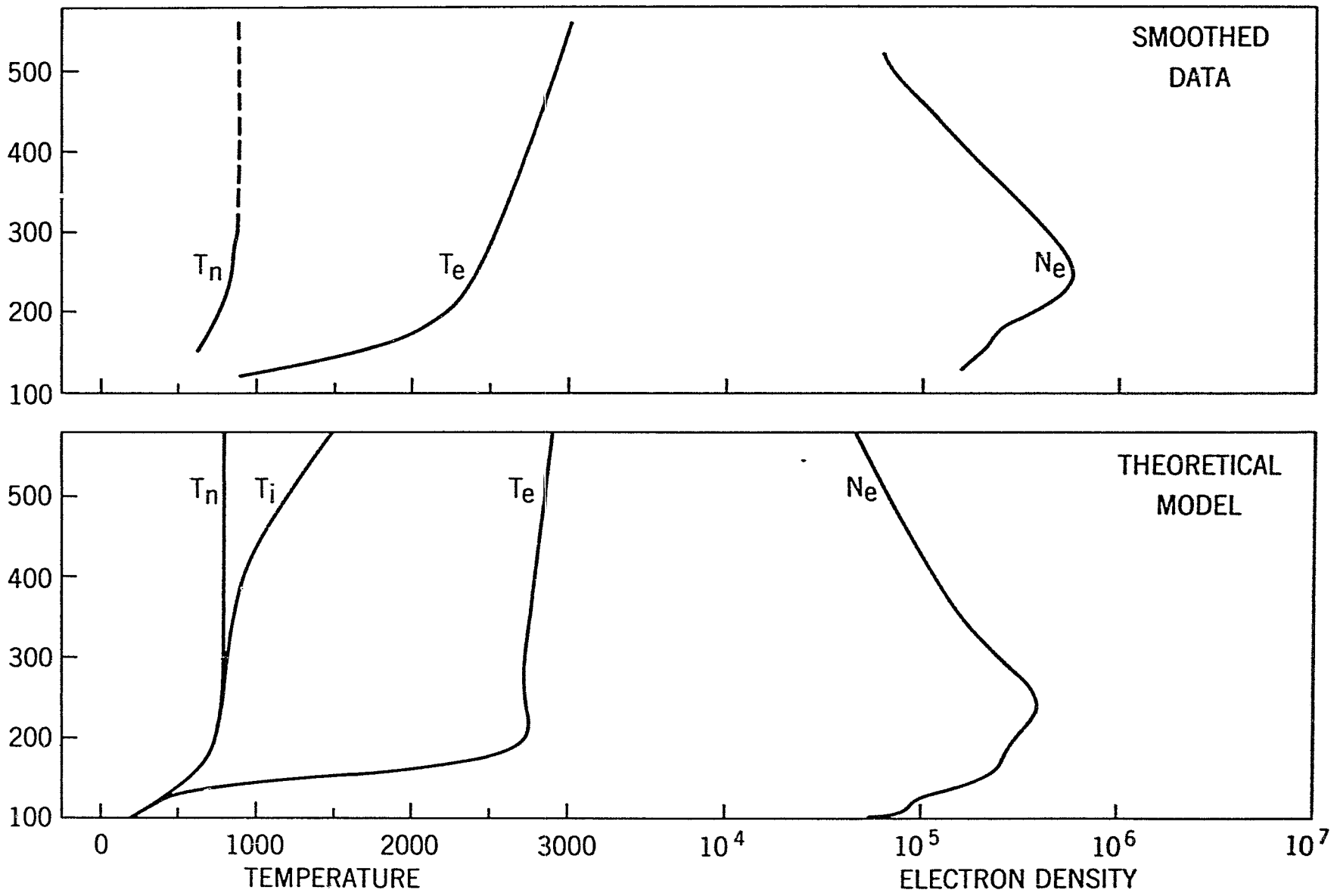

Figure 2.

SOLAR CYCLE VARIATION OF T_n, T_e AND N_e

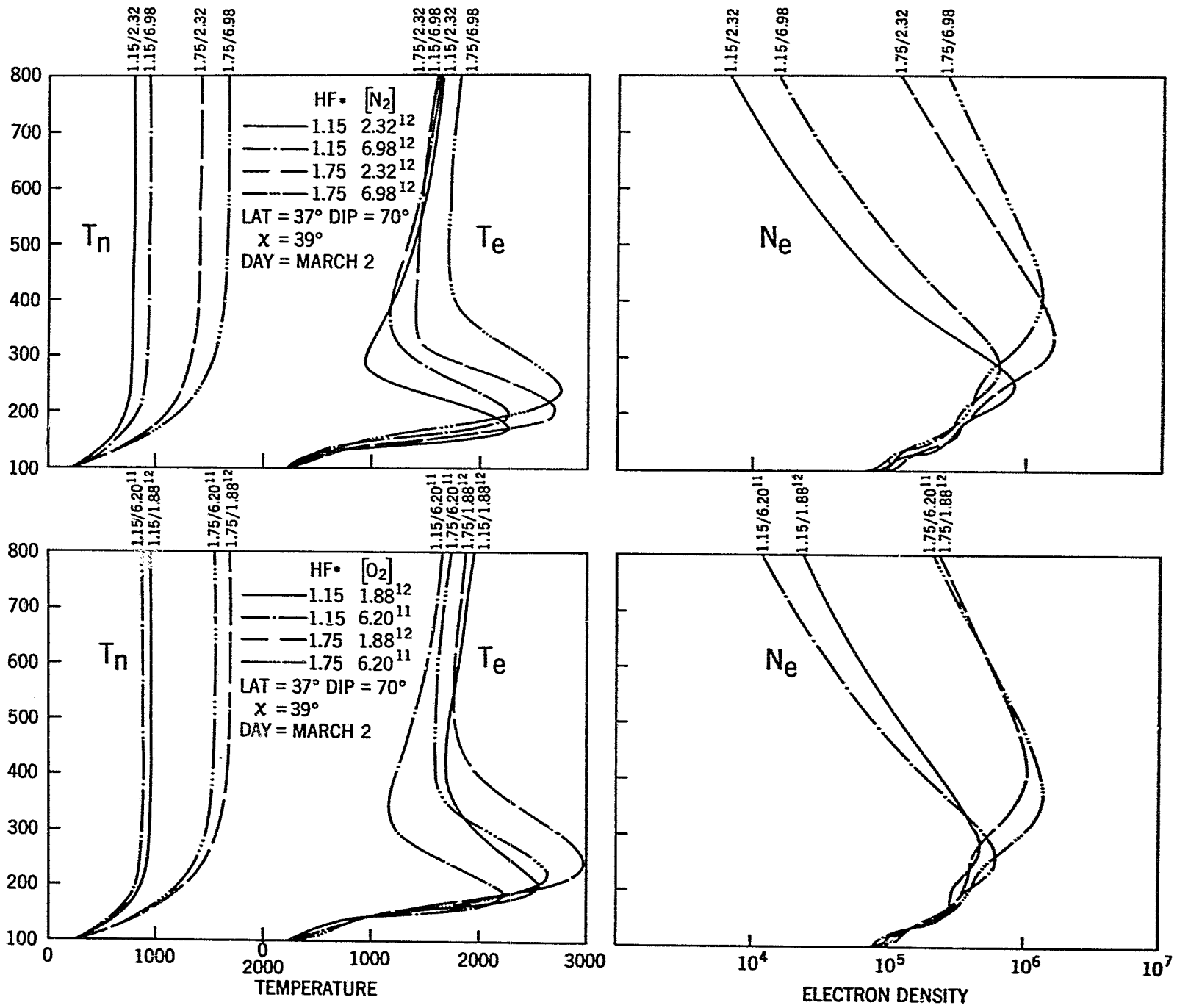

Figure 3.

SOLAR CYCLE VARIATION OF T_n, T_i, T_e, AND N_e

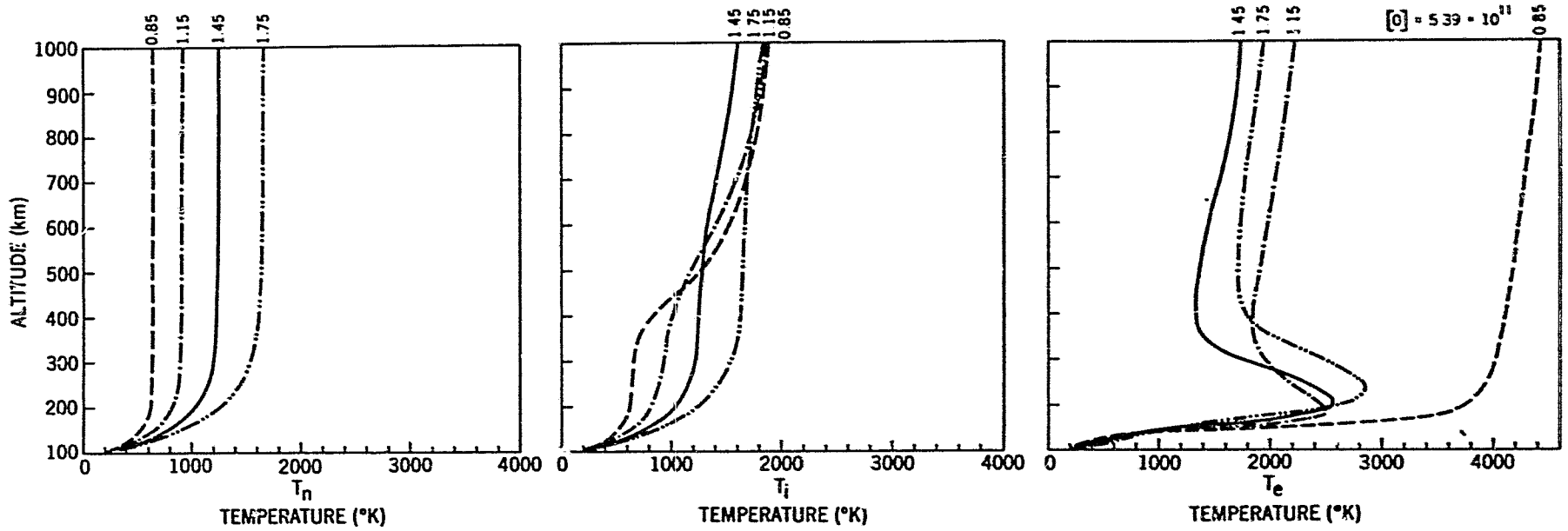

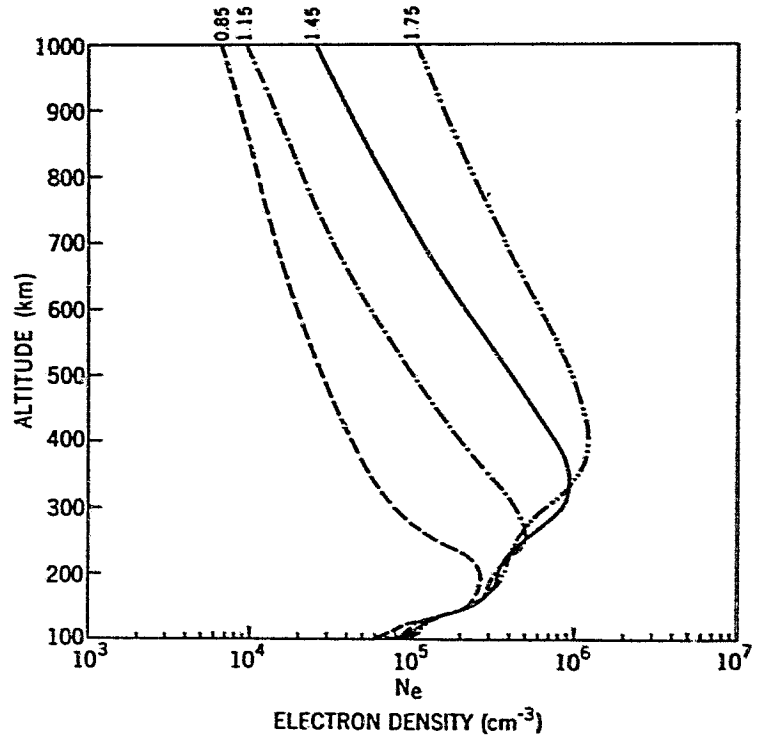

	$[N_2]$	$[O_2]$	$[O]$	$[He]$	$[H]$
BC =	4.65^{12},	1.25^{12},	5.39^{11},	2.50^{8},	1.00^{5}

LAT = 37° DIP = 70°

X = 39° DAY = MARCH 2

MF* = 0.85, 1.15, 1.45, 1.75

Figure 4.

SOLAR CYCLE VARIATION OF Tn, Ti, Te AND Ne

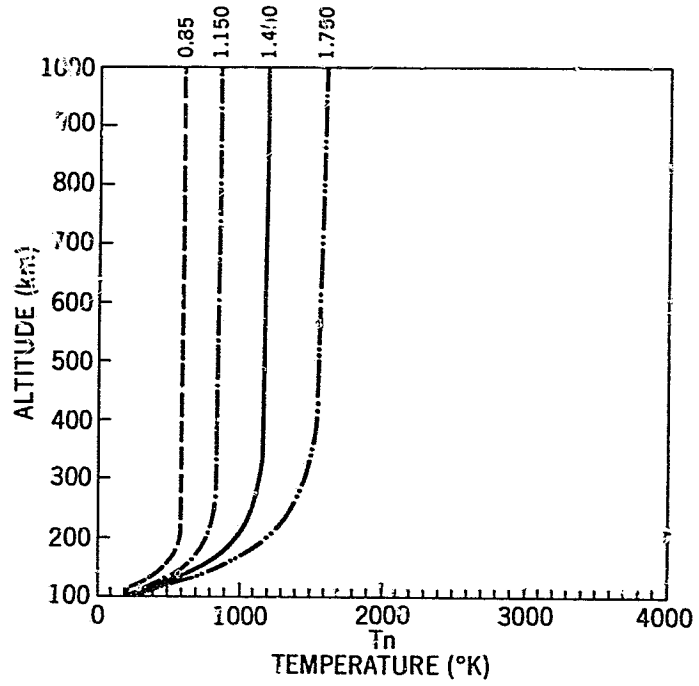

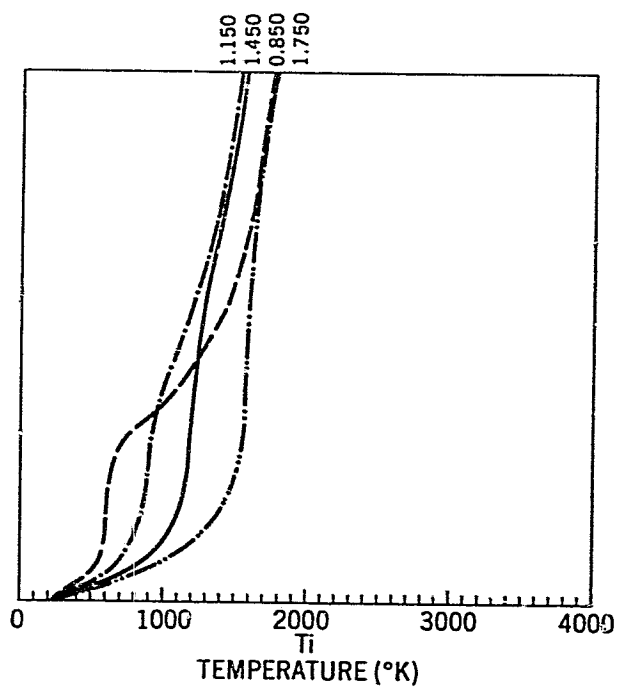

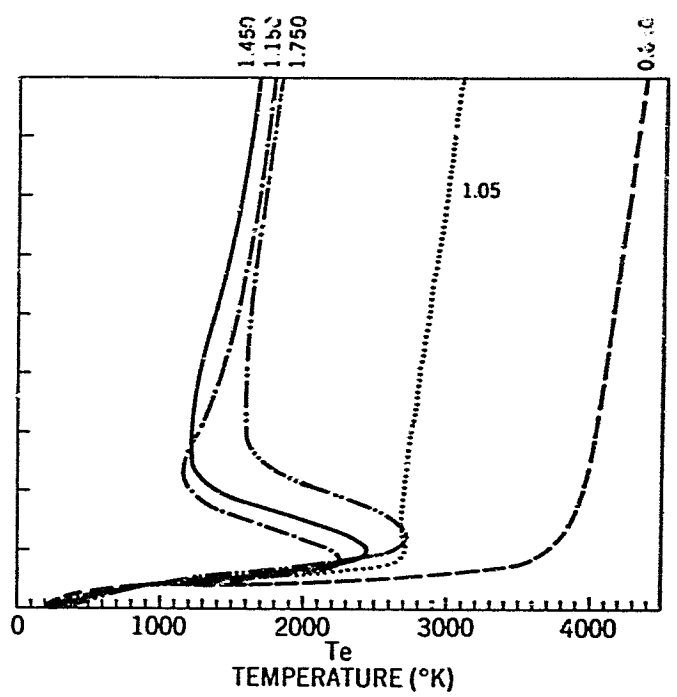

$[N_2]$ $[O_2]$ $[O]$ $[He]$ $[H]$

BC =4.65^{12}, 1.25^{12}, 6.75^{11}, 2.50^{8}, 1.00^{5}

LAT=37° DIP=70°

X =39° DAY=MARCH 2

HF *=0.85, 1.15, 1.45, 1.75

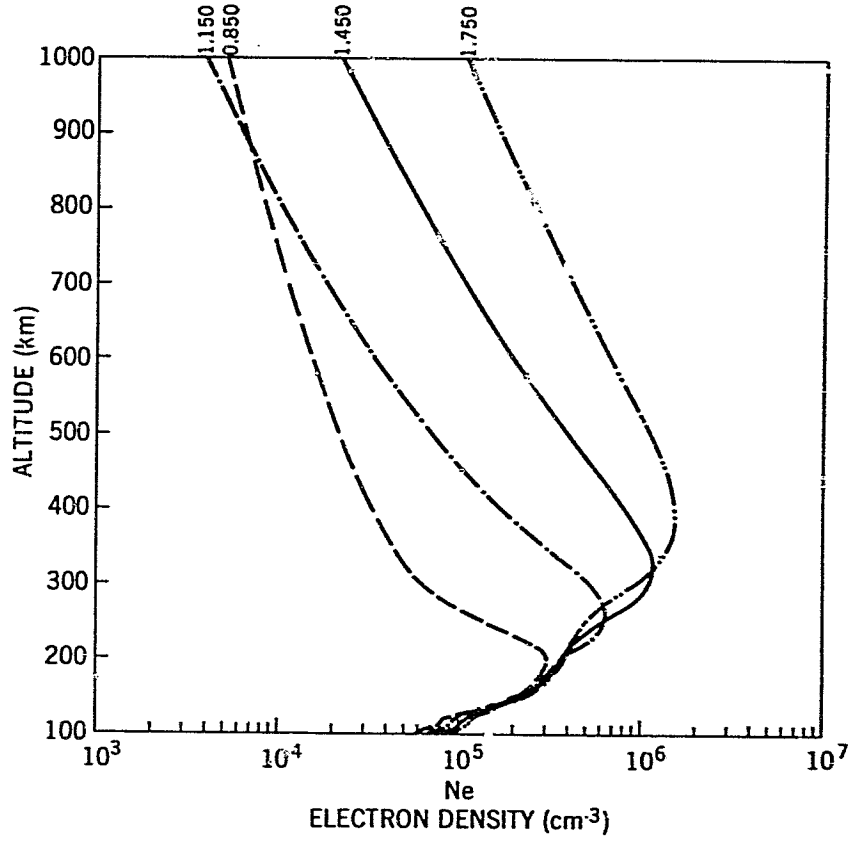

Figure 5.

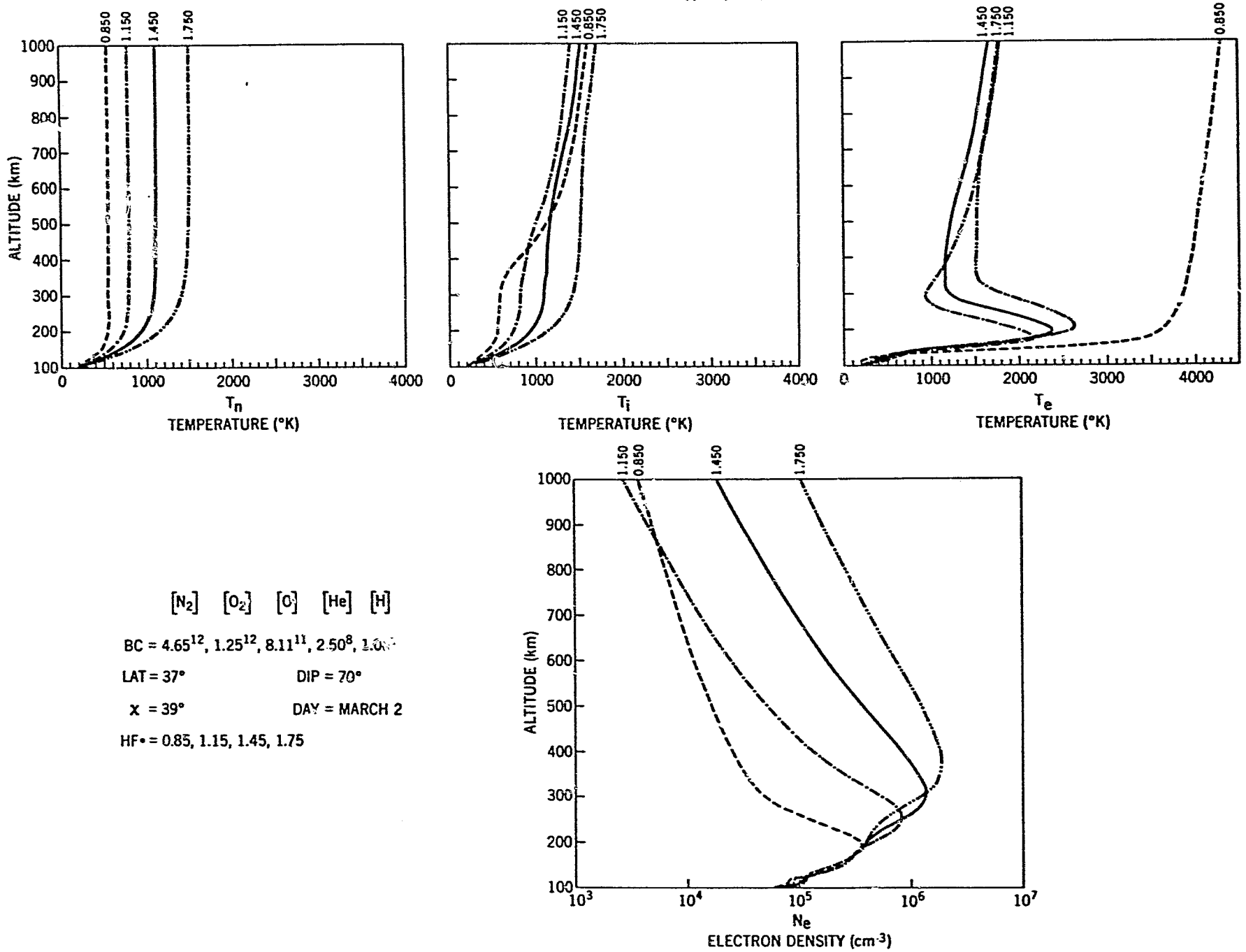

$[N_2]$ $[O_2]$ $[O]$ $[He]$ $[H]$

BC = 4.65^{12}, 1.25^{12}, 8.11^{11}, 2.50^{8}, 1.0[illegible]

LAT = 37° DIP = 70°

X = 39° DAY = MARCH 2

HF• = 0.85, 1.15, 1.45, 1.75

Figure 6.

SOLAR CYCLE VARIATION OF T_n, T_i, T_e, AND N_e

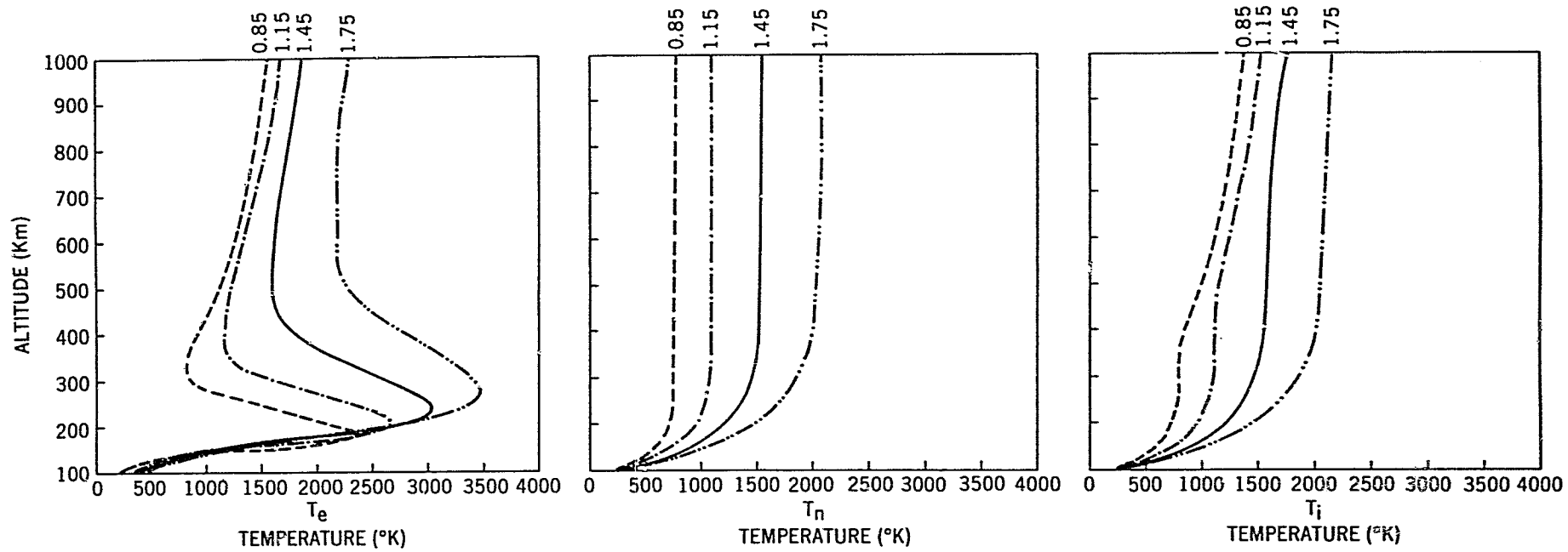

$[N_2]$ $[O_2]$ $[O]$ $[H_e]$ $[H]$

BC = 4.65^{12}, 1.25^{12}, 5.39^{11}, 2.50^{8}, 1.00^{5}

LAT = 18, Dip=50°

χ = 20° DAY=MARCH 2

MF* 0.85, 1.15, 1.45, 1.75

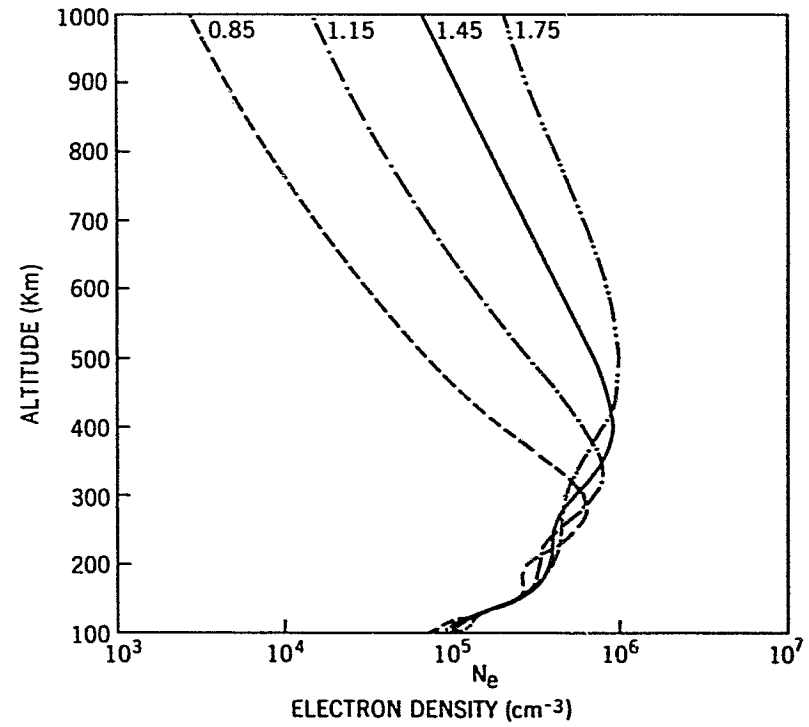

Figure 7.

SOLAR CYCLE VARIATION OF T_n, T_i, T_e AND N_e

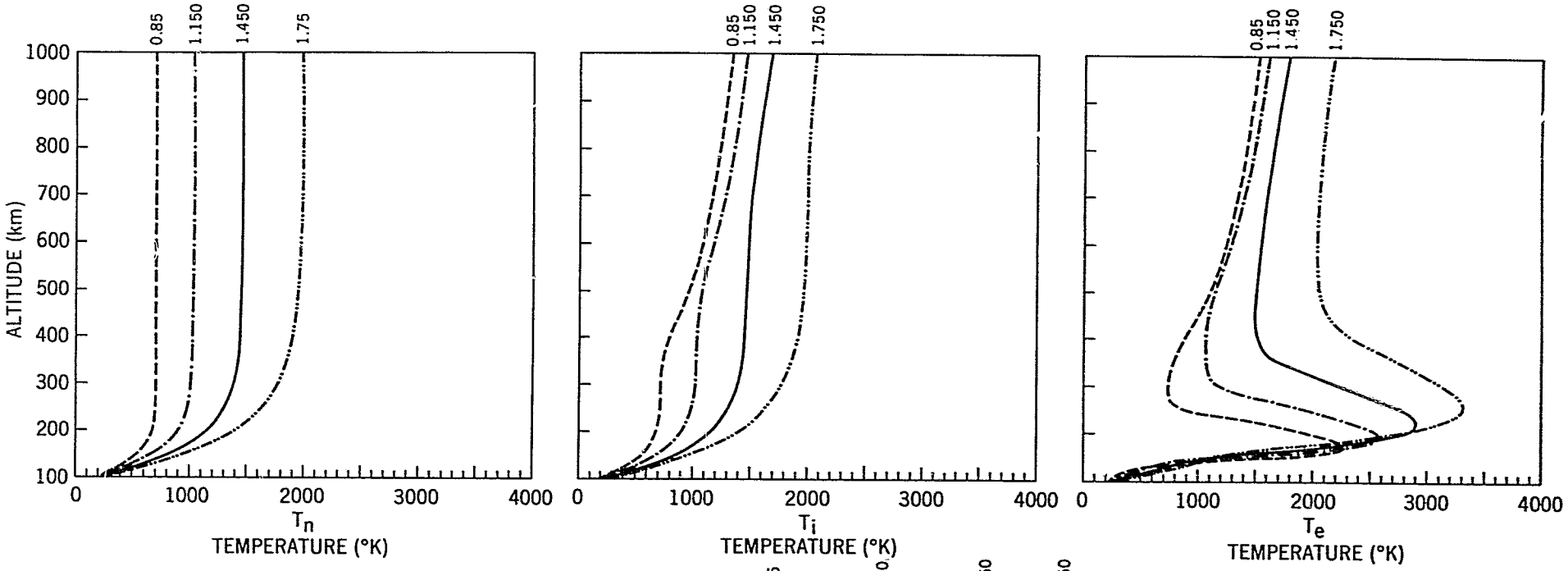

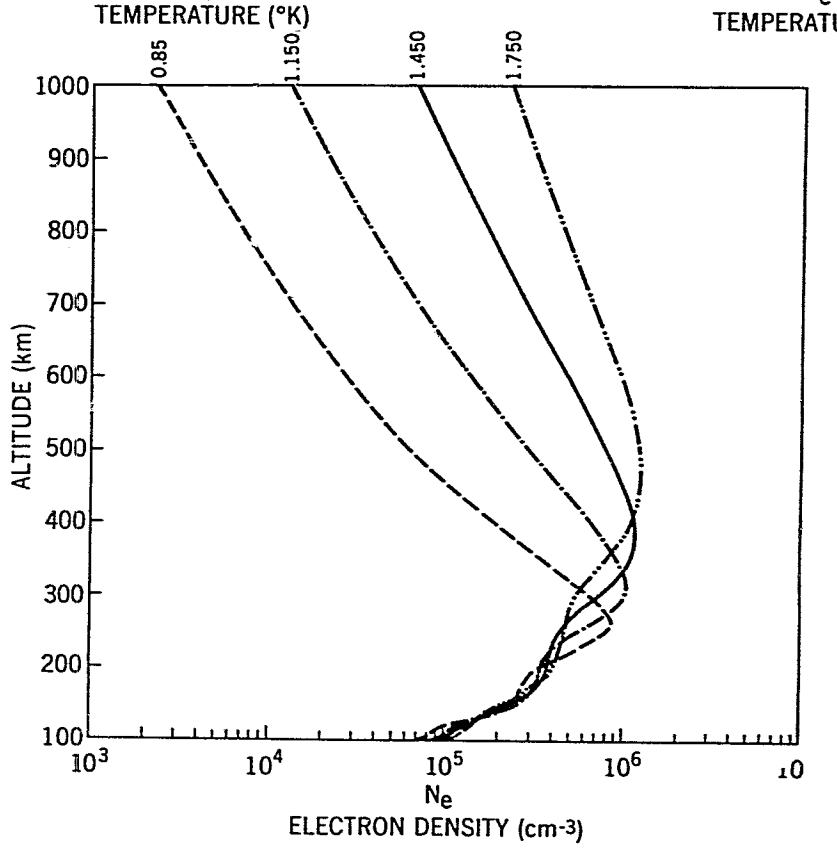

	$[N_2]$	$[O_2]$	[O]	[He]	[H]
BC =	4.65^{12},	1.25^{12},	6.75^{11},	2.25^{8},	1.00^{5}

LAT=18° DIP=50°

X =20° DAY=MARCH 2

HF*=0.85, 1.15, 1.45, 1.75

Figure 8.

SOLAR CYCLE VARIATION OF T_n, T_i, T_e, AND N_e

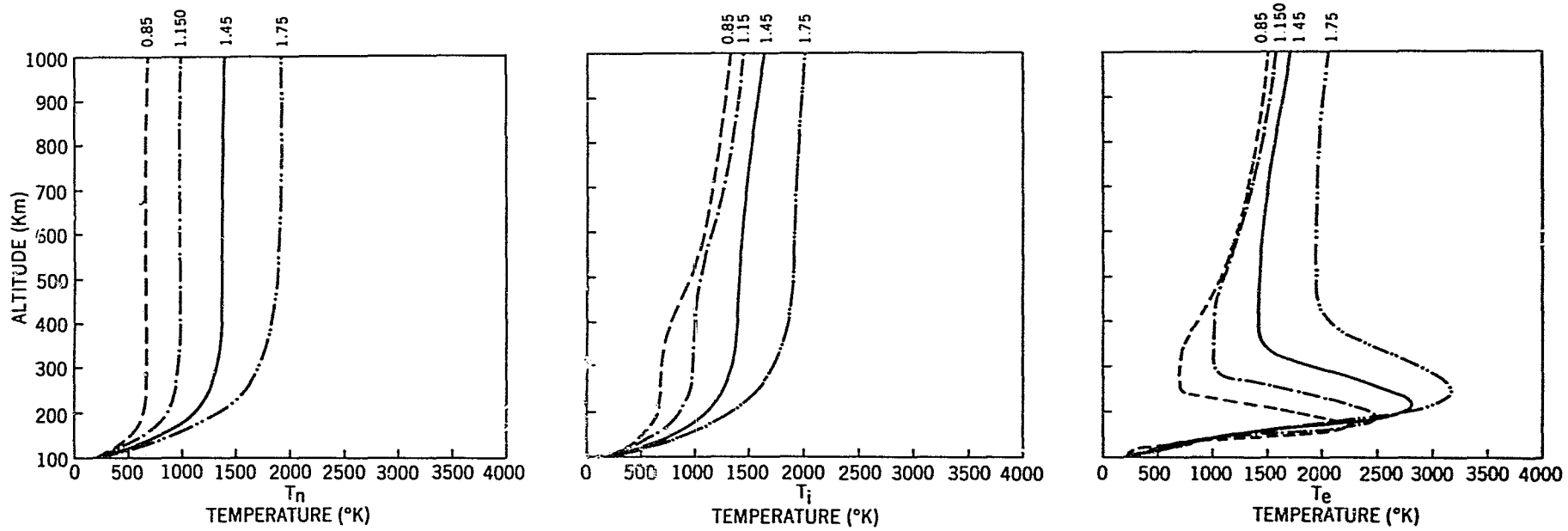

$[N_2]$ $[O_2]$ $[O]$ $[H_e]$ $[H]$

BC = 4.65^{12}, 1.25^{12}, 8.11^{11}, 2.50^{8}, 1.00^{5}

LAT = 18° DIP=50

χ = 20° DAY=MARCH 2

HF* 0.85, 1.15, 1.45, 1.17

Figure 9.

SOLAR CYCLE VARIATION OF T_n, T_i, T_e AND N_e

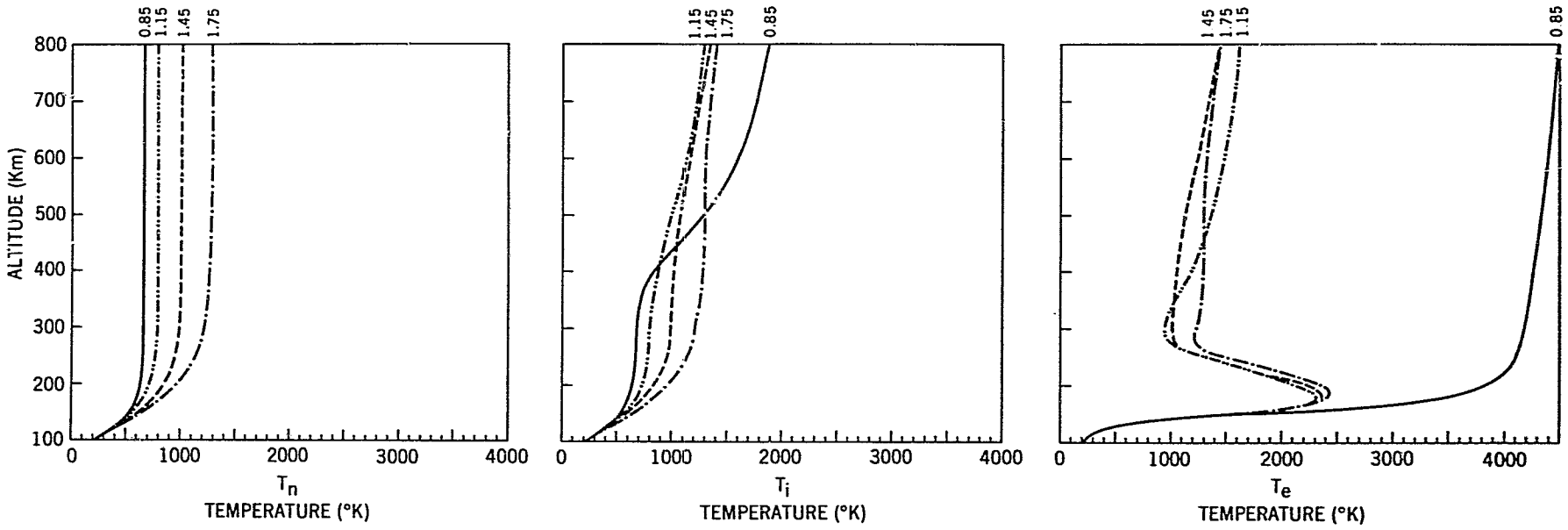

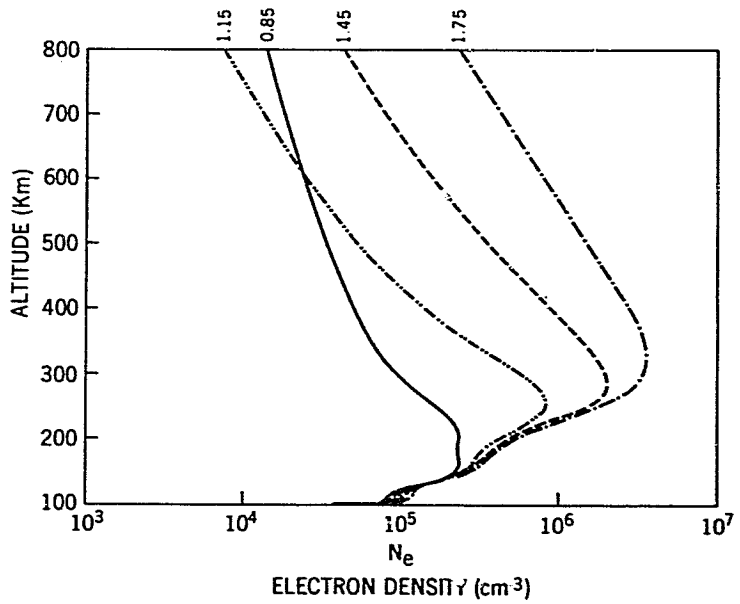

$[N_2]$ $[O_2]$ $[O]$ $[He]$ $[H]$

BC = 4.65^{12}, 1.25^{12}, VARIABLE, 2.50^{8}, 1.00^{5}

LAT = 37° DIP = 70°

χ = 39° DAY = MARCH 2

HF• = 0.85, 1.15, 1.45, 1.75

Figure 10.

SOLAR CYCLE VARIATION OF T_n, T_i, T_e, AND N_e

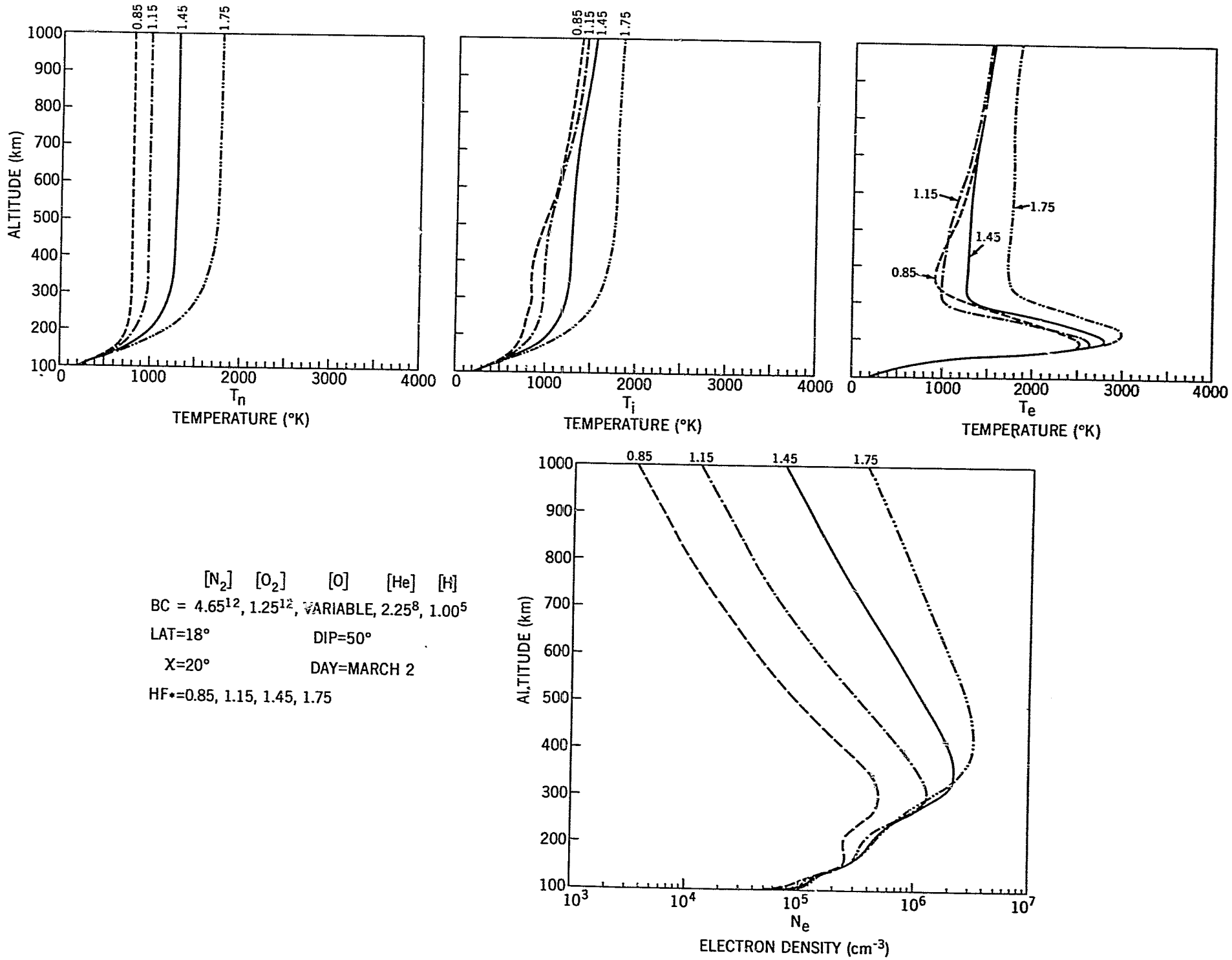

$[N_2]$ $[O_2]$ [O] [He] [H]

BC = 4.65^{12}, 1.25^{12}, VARIABLE, 2.25^{8}, 1.00^{5}

LAT=18° DIP=50°

X=20° DAY=MARCH 2

HF*=0.85, 1.15, 1.45, 1.75

Figure 11.